60th Annual Technical Conference Proceedings
Providence, Rhode Island, April 29-May 4, 2017
https://doi.org/10.14332/svc17.proc.42636

 ISSN 0737-5921
www.svc.org

Tribological Coatings for Improving Cutting Tool Performance

B. L. Strahin* and G. L. Doll
The University of Akron, Akron, OH USA

ABSTRACT

With an increasing usage of advanced high-strength steels, there is an escalating need for improvements in cutting tool performance for these alloys. In this study, the tribological performances of Cr_2N, WC/a-C:H, and Ti-MoS_2 coatings on AISI M2 steel were examined. Surface treatments were evaluated using dry pin-on-disk testing, Charpy impact testing, and a reciprocating impact-sliding test rig (RISTR) designed to replicate the interaction between cutting tools and high-strength steel sheet. Charpy testing of coated specimens showed no statistical change in impact toughness from the untreated steel. Pin-on-disk testing was performed to quantify the friction and wear of untreated and coated tool steel. These tests showed that Ti-MoS_2 coated tool steel had the lowest friction coefficient, and Cr_2N, the lowest wear rate. Impact tribometer testing showed that the Ti-MoS_2 coating yielded an increase of 370% in the number of cycles to failure over untreated specimens, while the WC/a-C:H coating was found to decrease the number of cycles to failure over untreated specimens. With an impact stress lower than the compressive yield strength of the AISI M2 steel, the fatigue life of the surface treatments scaled approximately as E^2/H^3, the inverse of the resistance to plastic deformation.

INTRODCTION

Background

Years of industry experience have revealed a growing need for new advancements in industrial cutting tools. Advanced-high strength steel (AHSS) exhibits a combination of strength and ductility not seen in traditional materials. Tool failures can cause costly downtimes in industry and can cause delays to first responders when cutting tools fail to cut through the AHSS frames used in modern automobiles [1]. Premature tool failure when cutting AHSS occurs from two primary mechanisms: increased wear and an increased risk of fracture [2]. This complicates the selection of cutting tool alloys because this must be balanced with the need for a higher strength material to shear the higher strength AHSS. Many manufacturers have used custom chemistries to obtain tooling that has a good combination of properties [3]. Success has also been seen when using tools manufactured from cermet, ceramic, and composite materials [4]. These materials can be very costly and lack the toughness required for cutting operations that see impact loading conditions. It was recently estimated that industrial cutting tools account for about $8 billion annually in developed markets [5]. An alternative to this approach is to engineer the surfaces of more common tools steels while providing the desired combination of wear resistance and strength in the cutting tool. Wear and damage on industrial tooling is caused by several different mechanisms. Theses mechanisms are adhesion, abrasion, diffusion between the tool and workpiece, thermal gradients, load variations, and impact loading [6]. Tool wear consists of both physical and chemical reactions and consists of approximately 50% abrasion, 20% adhesion, 10% chemical reaction, and 20% other [5]. Impacts to the tool cutting edge can cause cutting edge failure due to cracking, chipping, and plastic deformation [6]. Typically, cutting tools that have cracked or chipped cannot be resharpened and must be discarded. Adhesion can best be explained as friction welding between the two materials during contact. Chemical reactions can be reactions between workpiece and cutting tool, with lubricant, or with atmosphere. Traditionally, coatings with high hardness and high thermal stability have been used to provide wear resistance to industrial tooling. Industry trend has been to increase hardness of tool coatings to increase tool life [7]. Titanium nitride, titanium carbide, and aluminum oxide are recommended for dry cutting due to the higher temperatures generated [5] but chromium nitride, titanium-aluminum nitride, molybdenum disulfide, and amorphous hydrocarbon coatings have also been used [8,9]. Shear blades do not typically see the higher temperatures seen during dry machining and do not require coatings to combat this issue. Plasma nitriding has also seen some success in industrial cutting tools and has been shown to improve the percussive impact resistant of tool steels and decrease the adhesive wear due to sliding and impact [10]. Others have also shown that by reducing surface roughness and gas nitriding, the performance of lower cost steels can be improved enough to allow them to be used for tooling in place of higher cost materials [11]. However, these coatings are not suitable for all applications and often require lubrication to reduce friction and prevent failure [7,12], although the availability of lubrication in some cutting tool application is frequently low or non-existent.

In this study, coatings were deposited onto AISI M2 balls and impact tribometer specimens. Coatings of various hardness and elastic moduli values were selected for study. The goal of this study was to determine which coating properties have the largest impact of cutting tool life.

EXPERIMENTAL PROCEDURES

Coating Deposition

Candidate coatings were deposited by closed-field unbalanced magnetron sputtering onto AISI M2 substrates. The substrates consisted of 6 mm diameter balls and custom designed impact tribometer chisels. Chisel specimens were austenitized under vacuum at 1205 °C for 5 minutes, positive pressure (5 bar)nitrogen quenched to under 540 °C, cooled until warm to the touch, then double tempered at 540 °C for 2 hours (per temper)
to achieve a final hardness of 65 ±1 HRC. Prior to coating, the substrates were descaled, ultrasonically cleaned in an alkaline detergent, rinsed in deionized water, then hot air dried. After cleaning, substrates were immediately placed into the deposition chamber. The chamber was evacuated to a base pressure below 1x10-6 Torr prior to beginning the deposition process. High-purity (99.999%) argon gas was flowed into the chamber at 50 sccm for the duration of the deposition. A layer of approximately 100 nm of Cr was used as an adhesion layer for Cr_2N and WC/aC:H. A layer of approximately 100 nm of Ti was used as an adhesion layer for the Ti-MoS_2. Some of the properties of the coatings are tabulated in Table 1.

Table 1. Mechanical properties of selected coatings [7].

Coating	Hardness	Modulus	Thickness
Cr_2N	20 GPa	280 GPa	1.1 µm
Ti-MoS_2	7.9 GPa	172 GPa	1.4 µm
WC/aC:H	14 GPa	130 GPa	2.2 µm

Charpy Impact Testing

Charpy impact testing uses a striker to impact a specimen supported between two anvil-supports to produce a multi-axial stress with a high loading rate [13]. Although the components of crack initiation and crack propagation cannot be separated with a V-notch type specimen, Charpy impact testing can accurately predict brittle fracture when correlated with adequate service experience [14]. Charpy impact testing was completed using an Instron 600MPX (600 J) testing machine. Specimens were machine as standard Charpy V-Notch impact specimens and conformed to ASTM E23. Notches in all specimens were cut after heat treatment using a grinding wheel with the specified 45° angle and 0.25 mm radius. All specimens were tested at room temperature to simulate actual operating conditions of the cutting tools. Although Charpy impact testing is not a measurement of thin coatings, it was used to determine if the process used to deposit the coatings caused changes in the microstructure of the material that negatively affected its impact toughness, which is a key attribute of industrial tooling.

Wear Testing

Pin-on-disk testing was conducted with a CSEM High-Temperature Tribometer. Coatings were applied to 6-mm AISI M2 balls, with an average surface roughness prior to coating of Ra ~ 30 nm. The rotating disks were 50 mm diameter by 6 mm AR400 steel, with an average surface roughness of Ra ~ 200 nm that was selected to conform to the cutting tool environment. Tests were conducted with a 2 N load, producing a mean contact stress of 0.55 GPa, and 10 cm/s linear speed for 100m, 200m, and 400m distances. Wear scars were measured using a Zygo NewView 7300 3D optical profilometer with a 5X objective lens and 10X internal magnification. Wear volume of the balls was determined by subtracting a sphere of the initial radius from the worn ball. Wear volumes of the disks were calculated by using half the volume of an elliptical torus. Tests were conducted with a 2 N load, producing a mean contact stress of 0.55 GPa, and 10 cm/s linear speed for 100m, 200m, and 400m distances. Wear scars were measured using a Zygo NewView 7300 3D optical profilometer with a 5X objective lens and 10X internal magnification. Wear volume of the balls was determined by subtracting a sphere of the initial radius from the worn ball. Wear volumes of the disks were calculated by using half the volume of an elliptical torus.

Reciprocating Impact-Sliding Test Rig

The Reciprocating Impact-Sliding Test Rig (RISTR) was designed to simulate the extremely harsh tribological conditions seen by industrial cutting tools used to cut AHSS, such as rotary shear blades and scrap chopper knives. An Ingersoll-Rand 122Max pneumatic hammer regulated to operate at 620.5 kPa with a 19-mm diameter piston was used to impact high-strength steel test plates with specially designed chisel specimens.

Initial calculations for the design on the impact tribometer were performed using equations for general Hertzian contact. The equations for general Hertzian contact can be found in most texts on advanced engineering mechanics and applied elasticity. The mean and maximum contact stresses were calculated using Eq. 3.1 and Eq. 3.2, respectively.

$$\sigma_{c,mean} = \frac{\sqrt[3]{F}}{\pi c_a c_b \left(\frac{3(1-\nu)^2}{E\left(\frac{1}{r_1}+\frac{1}{r_1'}+\frac{1}{r_2}+\frac{1}{r_2'}\right)} \right)^{\frac{2}{3}}} \quad \text{Eq. 3.1}$$

$$\sigma_{c,max} = 1.5\sigma_{c,mean} \quad \text{Eq. 3.2}$$

where r_1 and r_1' are the radii in the planes perpendicular to the plane of contact of the first surface and r_2 and r_2' are the radii in the planes perpendicular to the plane of contact of the second surface. In the above equations, c_a and c_b are constants determined from the calculation of α from Table 3.3 in Ugural and Fenster's text (p. 169) [15]. The calculation of α is performed using Eq. 3.3.

$$\alpha = \cos^{-1}\left(\frac{\left[\left(\frac{1}{r_1}-\frac{1}{r_1'}\right)^2 + \left(\frac{1}{r_2}-\frac{1}{r_2'}\right)^2 + 2\left(\frac{1}{r_1}-\frac{1}{r_1'}\right)\left(\frac{1}{r_2}-\frac{1}{r_2'}\right)\cos 2\theta \right]^{\frac{1}{2}}}{\left(\frac{1}{r_1}+\frac{1}{r_1'}+\frac{1}{r_2}+\frac{1}{r_2'}\right)} \right) \quad \text{Eq. 3.3}$$

Variables were chosen to simulate the conditions that the cutting tools would endure during the most extreme operating conditions. The radii of the material being cut were taken as ∞ to represent a flat surface giving $1/r_2$ and $1/r'_2$ values of zero. The values used for the maximum and minimum curvatures for the cutting tool were the measured radius of a typical knife hub, r_1=89 mm, and the measured radius of the cutting tool curvature, r'_1=351 mm. The angle between the primary axes, Θ, was taken as 90°. Substituting these values into Ugural and Fenster's Table 3.3 gives an α=53.5°, and from linear interpolation, c_a=1.654 and c_b=0.630. A standard Poisson's ratio and elastic modulus for steel were assumed; i.e. ν=0.3 and E=200 GPa. The impact load was selected to be the force necessary to cut a piece of AHSS material with thickness (t) of 3 mm and a helix (or rake) angle of 15°. Using trigonometric relationships, the width (w) of the material being cut was found to be (3mm)/tan(15°), or 11 mm. The force required to cut AHSS with these dimensions can be calculated from the shear force calculation;

$$F = C_1 \sigma_{UT} t w \qquad \text{Eq. 3.4}$$

where C_1 is a ductility coefficient and σ_{UT} is the ultimate tensile strength [16]. The value for C1 typically falls between 0.65 and 0.85, with higher numbers being used for more ductile materials. The value for C_1 is assumed to be 0.85 due to the highly ductile nature of AHSS. Using data from industry updates gives σ_{UT} = 2.1 GPa. Substituting these values into Eq. 3.4 gives F = 60 kN. This force generates a mean contact stress of 1.8 GPa and a maximum contact stress of 2.7 GPa on the cutting tool.

The next step in the design was to determine the radius of the spherical tip on the chisel specimen that would be required to produce an equivalent contact stress during the testing. This was done by calculating the contact stress of a sphere on a flat plate. The calculations were completed using a mean contact stress of 1.8 GPa and calculating for the radius of the spherical tip. The calculation yielded a tip radius of 4.6 mm assuming a Poisson's ratio of 0.3 and equivalent elastic moduli for both materials.

Coated AISI M2 chisels impacted flat plates manufactured from AR400 steel that were situated at a -15° angle and were allowed to rotate upon impact to an angle of 0°. This rotation was critical to a design that could accurately simulate operating conditions during shearing of the material. The angle of rotation introduced a sliding element to the RISTR. In these applications, all cutting tools undergo sliding during shearing of the materials being cut. The angle was chosen based on geometrical layouts to determine the angle that the tooling is engaged in the cut on a rotary cutter such as a drum shear or scrap chopper, although any type of cutting tool will see significant amounts of sliding during use. During sliding contact, the shear stress produced is a function of the coefficient of friction and the contact stress produced. For this reason, it was suspected that the coefficient of friction might play a large part in tool life. This would be especially true in situations where the cutting tools cannot be lubricated or are not lubricated adequately. Using trigonometric relationships, the desired sliding distance was calculated to be 8.13 mm. With an impact frequency of 3,500 impacts per minute, the horizontal velocity was determined to be 0.47 m/s. The vertical velocity was analyzed using the same approach. Vertical travel was calculated to be 18.61 mm, producing a vertical velocity of 1.09 m/s. Figure 1 shows the diagram used for sliding calculations with chisel detail.

The impact tribometer was equipped with a flow controller, pressure regulator, and in-line air tool lubricator to ensure consistent performance throughout the entire testing duration. The finished tribometer is shown in Figure 2.

Impact tests were performed with 5,000-cycle intervals, and the spherical tips of each specimen were examined using an optical profilometer before and after each interval. A specimen was determined to have failed from plastic deformation if the radius of the tip exceeded 9mm. Any evidence of chipping, cracking, or spalling on the spherical tip after a test interval was also considered as a failure. Special attention was paid to pre-existing defects to prevent a specimen being deemed as failed from an initial flaw. A new plate was installed after 100,000 impacts as well as for each new chisel specimen.

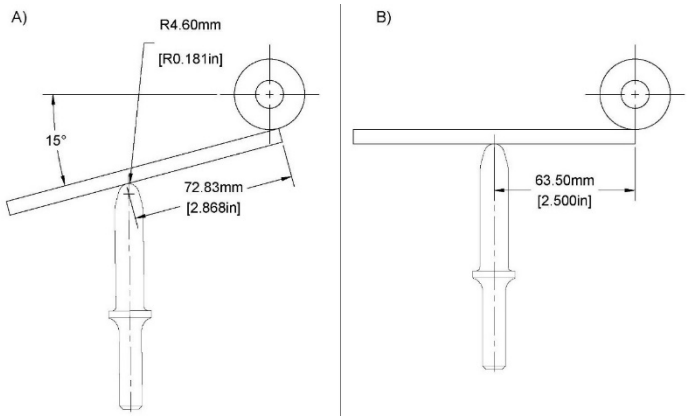

Figure 1. Diagram of the RISTR showing chisel geometry and a graphical representation of the sliding calculations showing A) initial position and B) end of stroke position.

RESULTS AND DISCUSSION

Impact Results

All specimens showed a Charpy impact energy of approximately 2.2 J. The data clearly show that there was no significant change in impact energy from the application of the engineered surfaces. This indicates that the coating deposition processes did not cause positive or negative changes to the combined impact toughness of the coating and substrate of the combinations tested. Figure 3 shows the average impact energies obtained from Charpy impact testing.

The data collected from RISTR testing show improvements from the M2 baseline results for the Ti-MoS_2 (~370%) and Cr_2N (~58%) coated chisels. RISTR testing agrees with research by others that reported soft coatings demonstrate a more significant improvement than hard coating at very high loads [17]. M2, Cr_2N, and Ti-MoS_2 failed due to spalling of the substrate, causing failure of the coating on coated specimens. Ti-MoS_2 also had cracking originating at the site of the spall. This is most likely caused by surface fatigue from the high contact stresses. Conversely, an ~86% decrease in cycles to failure was observed for the WC/a-C:H coated specimens. The WC/a-C:H results are consistent with previously performed research that reported delamination due to brittle fracture of the coating began to occur at stresses of 2.25 GPa, a value less than that used in these tests ($\sigma_{c,max}$ = 2.8 GPa) [18]. Solid plots of failures for each coating type are shown in Figure 4 and Figure 5 shows the average cycles to failure from RISTR testing for each coating tested.

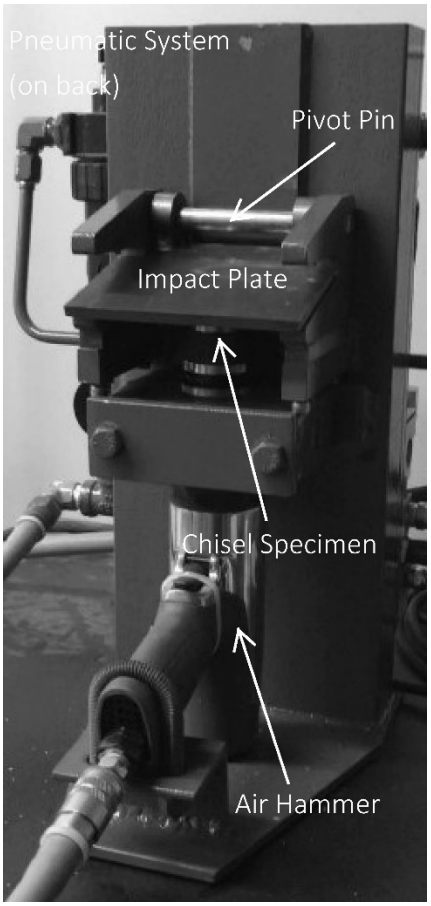

Figure 2. Photograph of the RISTR with specimen loaded.

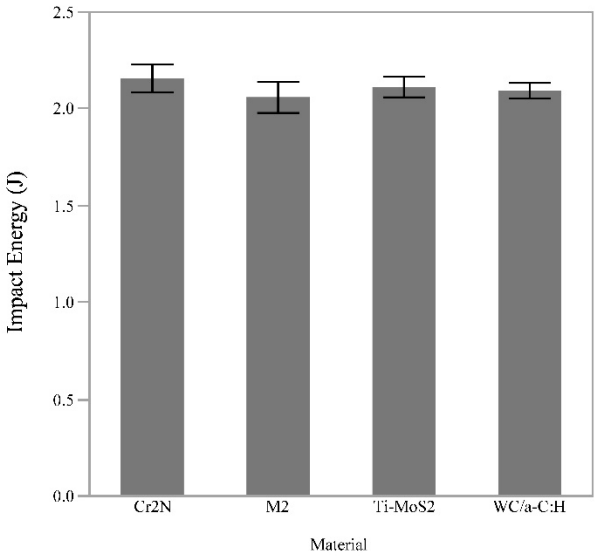

Figure 3. Average impact energies obtained from Charpy impact testing.

Further examination of the data in Fig. 5 revealed a correlation between cycles to failure and the resistance of the coating to plastic deformation. The resistance to plastic deformation is defined as

$$R_{Plastic} = \frac{H^3}{E^2} \qquad \text{Eq. 4.1}$$

where H is the hardness of the coating and E is the elastic modulus of the coating [19]. As the resistance to plastic deformation decreases, the number of cycles to failure increases.

This suggests that coatings selected for cutting tools subjected to impact should have a low resistance to plastic deformation. A graphical representation of this relationship is shown in Fig. 6, and the data can be described by

$$N_{failure} = A\left(\frac{H^3}{E^2}\right)^{-1} + B \qquad \text{Eq. 4.2}$$

where A and B were determined to be 3,986 GPa and 11,306, respectively.

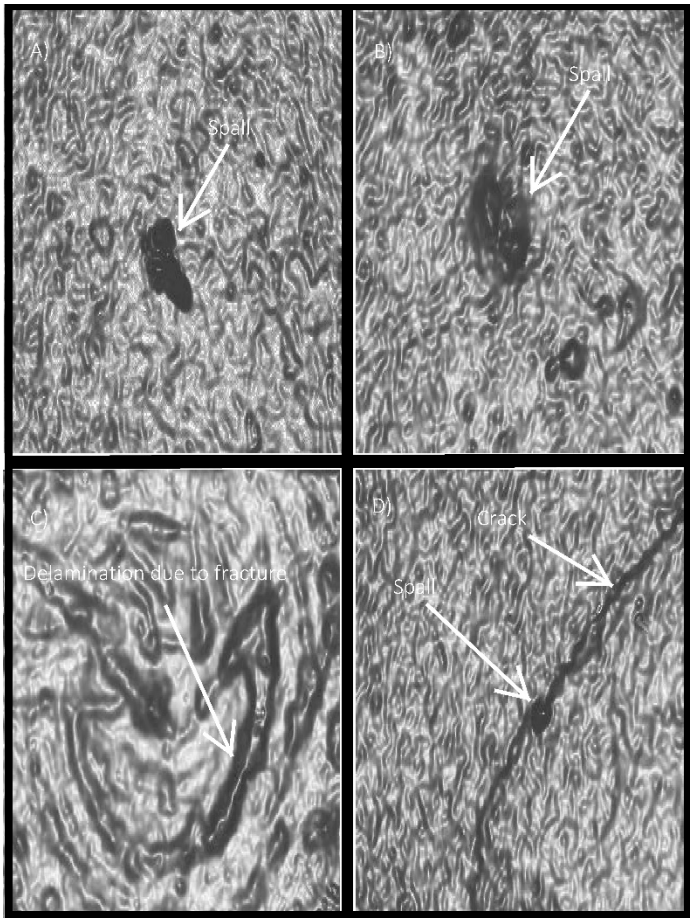

Figure 4. Solid plots of each coating failure showing the A) spallation of M2, B) spallation of Cr_2N specimen, C) the delamination of WC/aC:H, and D) spallation and cracking of Ti-MoS_2.

Friction and Wear

Friction coefficients were measured in unidirectional sliding in dry contact for four materials pairings. Figure 7 shows the average values of the friction for each of the distances tested. The data show that although the tests wore though the coatings completely, both WC/aC:H and Ti-MoS_2 continued to provide some lubricity after coating failure and allowed the system to operate at a lower friction than the M2/AR400 pairing. These observations are in agreement with Rechberger et. al. that stated that soft coatings can continue to provide improvement during operation even though only an extremely thin, almost non-existent layer remains [17].

Figure 8 shows wear volume (mm^3) of the ball for each pairing plotted against dissipated energy (J). Dissipated energy (E_d) was calculated by

$$E_d = \mu F d \qquad \text{Eq. 4.3}$$

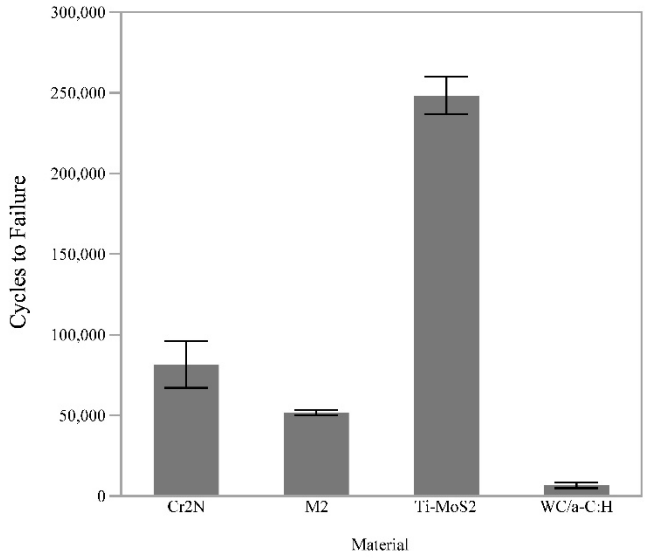

Figure 5. Average cycles to failure for each surface.

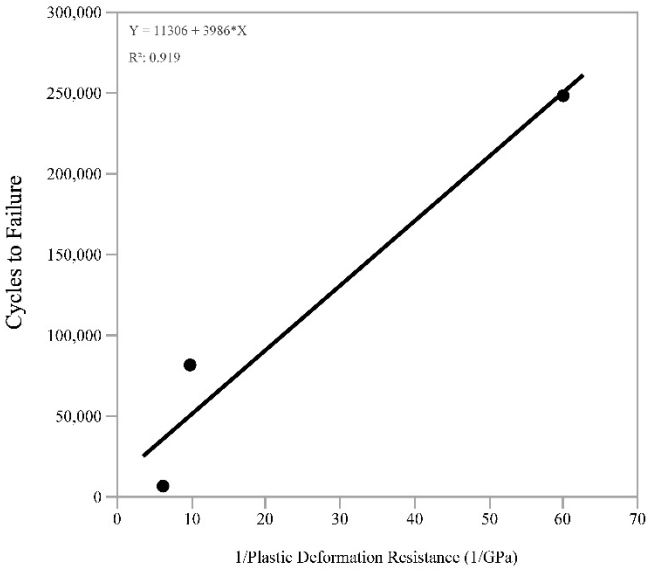

Figure 6. Graphical representation of the correlation between cycles to failure and the resistance of the coating to plastic deformation.

where μ is the coefficient of friction and d is the sliding distance.

Values of the slopes (α) of the best linear fits to the data were $5.44x10^{-8}$ mm^3/J (Cr_2N), $5.96x10^{-7}$ mm^3/J (WC/a-C:H), $7.57x10^{-7}$ mm^3/J (M2), and $8.23x10^{-7}$ mm^3/J (Ti-MoS_2). The α-values, or wear coefficients, scaled with the hardness of chisel surface (H = 8.2 GPa for M2 steel). Within the Archard formalism, wear volume (V) is related to dissipated energy and surface hardness as

$$V = k\left(\frac{E_d}{H}\right) \qquad \text{Eq. 4.4}$$

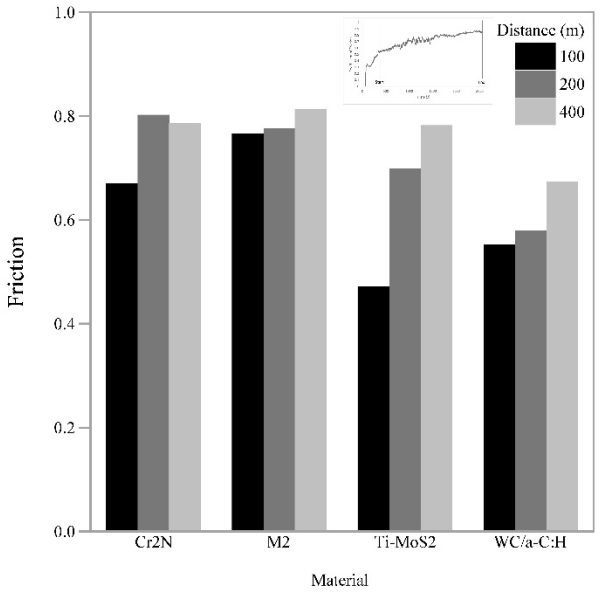

Figure 7. Friction coefficients for each material pair. The inset is representative of the region from which the steady-state friction was taken for each test.

Evaluation of the collective results from the wear and impact testing indicated that the ability of the coating to accommodate plastic deformation was the most critical attribute for a coating on M2 tool steel to cut AHSS. Although the Cr_2N coating provided significant wear resistance over untreated M2 steel, only minor improvements in cycles to failure were achieved with this coating. On the other hand, while the Ti-MoS_2 coating was less wear resistant than the untreated steel, it provided the largest increase in cycles to failure. Although both Ti-MoS_2 and WC/aC:H coatings had lower friction against AR400 than the untreated M2 balls, Ti-MoS_2 increased while WC/aC:H decreased the cycles to failure. This suggests that the friction coefficient has little impact on the number of cycles to failure.

CONCLUSIONS

The advancements of AHSS have created many obstacles that can cause costly downtime or create delays during emergency situations. The application of coatings on tool steels can provide a viable option for simultaneously optimizing wear resistance and strength. Of the coatings tested in this study, Ti-MoS_2 provided the most significant increase in cycles to failure when tested in an impact tribometer designed to replicate an actual application of cutting AHSS sheets. Based upon the results of this study, several conclusions can be made;

- A lower resistance to plastic deformation (low H^3/E^2) of the coating had the largest impact in increasing the cycles to failure in impact-sliding conditions seen in industrial cutting tools.

- Although wear resistance is necessary for extended operation of cutting tools, it is not the most important coating property for extending tool life.

- An ideal tool coating would have as high of a toughness as possible to reduce cracking and extend tool life, i.e. best possible combination of high ductility (low resistance to plastic deformation) and a high hardness (good wear resistance).

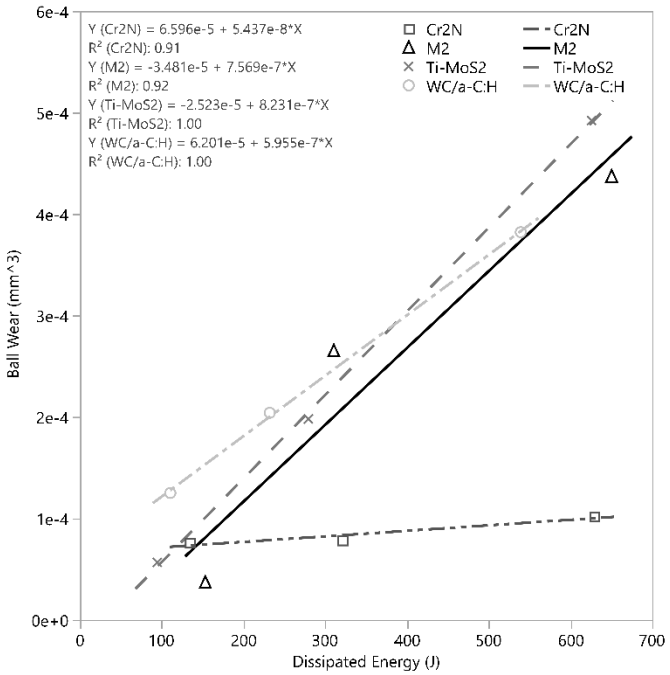

Figure 8. Plot of dissipated energy and ball wear used to determine wear coefficients.

ACKNOWLEDGEMENTS

The authors would like to thank Butech Bliss and Akron Research and Technology for their funding of this research.

REFERENCES

[1] J. Van Rensselar, The Riddle of Steel: A-UHSS, Tribol. Lubr. Technol. (2011) 38–46.
[2] M. Pinkham, Tollers Tooling Up for High-Strength Steel, Met. Cent. News. (2014) 18–24.
[3] T. Triplett, Ahead of the AHSS Curve, Met. Cent. News. (2013) 26–29.
[4] A. Altin, M. Nalbant, A. Taskesen, The effects of cutting speed on tool wear and tool life when machining Inconel 718 with ceramic tools, Mater. Des. 28 (2007) 2518–2522. doi:10.1016/j.matdes.2006.09.004.
[5] J. Kopac, Influence of cutting material and coating on tool quality and tool life, J. Mater. Process. Technol. 78 (1998) 95–103.
[6] A. Braghini Junior, A.E. Diniz, F.T. Filho, Tool wear and tool life in end milling of 15–5 PH stainless steel under different cooling and lubrication conditions, Int. J. Adv. Manuf. Technol. 43 (2009) 756–764. doi:10.1007/s00170-008-1744-6.

[7] J. Rechberger, R. Dubach, Soft physical vapour deposition coatings - a new coating family for high performance cutting tools, Surf. Coat. Technol. 60 (1993) 584–586.
[8] S. Chinchanikar, S.K. Choudhury, Evaluation of Chip-tool Interface Temperature: Effect of Tool Coating and Cutting Parameters during Turning Hardened AISI 4340 Steel, Procedia Mater. Sci. 6 (2014) 996–1005. doi:10.1016/j.mspro.2014.07.170.
[9] A. Devillez, F. Schneider, S. Dominiak, D. Dudzinski, D. Larrouquere, Cutting forces and wear in dry machining of Inconel 718 with coated carbide tools, Wear. 262 (2007) 931–942
. doi:10.1016/j.wear.2006.10.009.
[10] M.U. Devi, O.N. Mohanty, Plasma-nitriding of tool steels for combined percussive impact and rolling fatigue wear applications, Surf. Coat. Technol. 107 (1998) 55–64.
[11] D. Toboła, W. Brostow, K. Czechowski, P. Rusek, Improvement of wear resistance of some cold working tool steels, Wear. 382–383 (2017) 29–39. doi:10.1016/j.wear.2017.03.023.
[12] B. Podgornik, B. Zajec, N. Bay, J. Vižintin, Application of hard coatings for blanking and piercing tools, Wear. 270 (2011) 850–856. doi:10.1016/j.wear.2011.02.013.
[13] ASTM E23-12c, Standard Test Methods for Notched Bar Impact Testing of Metallic Materials, in: ASTM Book Stand., ASTM International, West Conshohocken, PA, 2012.
[14]Impact Toughness Testing, in: Mech. Test. Eval., ASM International, Materials Park, OH, 2000: pp. 596–611.
[15] A. Ugural, S. Fenster, Contact Stresses, in: Adv. Mech. Mater. Appl. Elast., 5th ed., Prentice Hall, Westford, MA, 2013: pp. 159–170.
[16] J. Schey, Shearing, in: Introd. Manuf. Process., 3rd ed., McGraw-Hill, 2000: pp. 388–397.
[17] J. Rechberger, P. Brunner, R. Dubach, High performance cutting tools with a solid lubricant physically vapour-deposited coating, Surf. Coat. Technol. 62 (1993) 393–398.
[18] B. Mahmoudi, B. Tury, C.H. Hager, G.L. Doll, Effects of Black Oxide and a WC/a-C:H Coating on the Micropitting of SAE 52100 Bearing Steel, Tribol. Lett. 58 (2015). doi:10.1007/s11249-015-0494-5.
[19] A. Leyland, A. Matthews, eds., On the Significance of the H/E Ratio in Wear Control: A Matrix Composite Coating Approach to Optimized Tribological Behaviour, Wear. (2000) 1–11.

FOR FURTHER INFORMATION:

B. L. Strahin
The University of Akron,
Akron, OH USA
bls103@zips.uakron.edu